Effect of W self-implantation and He plasma exposure on early-stage defect and bubble formation in tungsten

M. Thompson[1], D. Drummond[1], J. Sullivan[1], R. Elliman[2], P. Kluth[2], N. Kirby[3], D. Riley[4], C. S. Corr[1]

[1] Plasma Research Laboratory, Research School of Physics and Engineering, Australian National University, Canberra
[2] Electronic Materials Engineering, Research School of Physics and Engineering, Australian National University, Canberra
[3] Australian Synchrotron, 800 Blackburn Road, Clayton, VIC 3168, Australia
[4] Australian Nuclear Science and Technology Organisation, Sydney

Abstract

To determine the effect of pre-existing defects on helium-vacancy cluster nucleation and growth, tungsten samples were self-implanted with 1 MeV tungsten ions at varying fluences to induce radiation damage, then subsequently exposed to helium plasma in the MAGPIE linear plasma device. Positron annihilation lifetime spectroscopy was performed both immediately after self-implantation, and again after plasma exposure.

After self-implantation vacancies clusters were not observed near the sample surface (<30 nm). At greater depths (30-150 nm) vacancy clusters formed, and were found to increase in size with increasing W-ion fluence. After helium plasma exposure in the MAGPIE linear plasma device at ~300 K with a fluence of 10^{23} He-m^{-2}, deep (30-150 nm) vacancy clusters showed similar positron lifetimes, while shallow (<30 nm) clusters were not observed. The intensity of positron lifetime signals fell for most samples after plasma exposure, indicating that defects were filling with helium. The absence of shallow clusters indicates that helium requires pre-existing defects in order to drive vacancy cluster growth at 300 K.

Further samples that had not been pre-damaged with W-ions were also exposed to helium plasma in MAGPIE across fluences from $1x10^{22}$ to $1.2x10^{24}$ He-m^{-2}. Samples exposed to fluences up to $1x10^{23}$ He-m^{-2} showed no signs of damage. Fluences of $5x10^{23}$ He-m^{-2} and higher showed significant helium-cluster formation within the first 30 nm, with positron lifetimes in the vicinity 0.5-0.6 ns. The sample temperature was significantly higher for these higher fluence exposures (~400 K) due to plasma heating. This higher temperature likely enhanced bubble formation by significantly increasing the rate interstitial helium clusters generate vacancies, which is we suspect is the rate-limiting step for helium-vacancy cluster/bubble nucleation in the absence of pre-existing defects.

1. Introduction

Modelling nano-scale modification of tungsten under helium, hydrogen and neutron exposure requires a detailed understanding of a large number of physical processes. For efficient computation of material modification on time and length scales relevant for ITER, these

nano-scale processes must be parameterised in such a way that they can be incorporated into higher scale models without the need to model them explicitly. This requires detailed atomistic modelling, typically with Monte-Carlo simulations performed on systems of hundreds or thousands of atoms [1–3], combined with empirical verification of those models to ensure that the conclusions are relevant in real materials that are invariably much larger and more complex.

The nucleation of helium bubbles in tungsten is a particularly important process as it lies at the interface between atomistic scale processes such as helium-vacancy binding and the mesoscopic scale of the helium bubbles themselves. Vacancy formation energies in the tungsten matrix are extremely high (~ 3 eV [4–6]), so thermally induced vacancy concentrations will be negligible for low temperature plasma exposure (< 700 K). Where vacancies do exist, helium binds very strongly to them, providing a nucleation site for vacancy-helium cluster growth and ultimately bubble formation [7].

Even without pre-existing vacancies it is energetically favourable for interstitial helium clusters to form, resulting in helium self-trapping [8]. As these clusters grow they are capable of bootstrapping their own vacancies by forcing tungsten out of their lattice sites [9], with the activation energy of this process decreasing with increasing size of the helium cluster [10]. The mobility of these structures is very sensitive to both the number of bound vacancies and helium atoms, and can change via the spontaneous creation or annihilation of Frenkel pairs [11]. Vacancy formation energies are significantly lower in the vicinity of the sample surface [12] and grain boundaries [13], leading to enhanced cluster formation in these regions.

Helium cluster induced vacancy formation is expected to be the dominant vacancy formation process in tungsten with few pre-existing defects due to the high vacancy formation energies. This occurs via “trap mutation” where the addition of helium to a helium-vacancy cluster leads to the ejection of a tungsten interstitial atom in order to accommodate the growing number of helium atoms, for instance through the reaction [14]:

$$V\mathrm{He}_n + He \rightarrow V_2\mathrm{He}_{n+1} + I \qquad (1)$$

Here, *V* represents a vacancy, and *I* a tungsten interstitial atom. As bubbles grow pressure builds within them, which in turn strains the surrounding tungsten matrix until the bubble is expanded via loop punching [15]. This process leads to a significant drop in the bubble’s internal energy, inhibiting the subsequent breakup of larger clusters.

Recent molecular dynamics modelling by Hammond *et al.* [16] also demonstrates that the crystallographic orientation of the surface can have a significant influence on helium-vacancy cluster properties, including the reflected fraction of helium incident on the tungsten surface, helium/vacancy ratios, the orientation of clusters, and the morphology of surface features. Notably, they found that near-surface bubbles were too small and their growth rates too slow to account for the fuzz-like structures that are known to form on tungsten under helium plasma, suggesting deeper bubbles must account for this phenomenon.

In ITER, and later DEMO, vacancy clusters induced by neutron irradiation could play a significant role in the nano-scale modification of tungsten. Positron annihilation lifetime spectroscopy performed on neutron-irradiated (110) single crystal tungsten by Hu *et al.* [17] shows the formation of many small defects (<10 vacancies), which agglomerated into larger structures after subsequent annealing at 400°C. Defect concentrations trended downward with annealing temperature as vacancy complex dissociation and defect recovery took place.

Extrapolating these findings to ITER is difficult as helium binds strongly to vacancy clusters and is known to stabilise them. To better understand the interplay between helium and radiation-induced defects we performed a series of experiments on helium plasma irradiated and 1 MeV self-implanted tungsten to determine how pre-existing defects affect vacancy cluster nucleation and growth in tungsten. We use a combination of positron annihilation lifetime spectroscopy (PALS) and grazing incidence small angle X-ray scattering (GISAXS) to measure early-stage defect formation. These techniques are complementary, as PALS is especially well suited to small vacancy clusters, while larger bubbles can be measured with GISAXS.

2. Measuring early-stage damage formation

To simulate the effects of neutron damage polycrystalline W samples (PLANSEE, 99.97 wt% W) were irradiated at room temperature with 1 MeV W ions to fluences ranging from $1.8x10^{15}$ m^{-2} to $5.4x10^{17}$ m^{-2}, which correspond to damage levels of 0.001 dpa (displacements per atom) and 0.3 dpa at a depth of 30 nm. Self-implantation was performed on an NEC (model 5SDH-4) 1.7 MV tandem ion accelerator at the Australian National University by scanning the ion beam across the sample surface. Damage levels were calculated by SRIM [18] using the methods outlined in [19] assuming a tungsten atom displacement energy of 90 eV as recommended in [20]. The projected range of implanted ions and vacancies generated as a function of depth are show in Figure 1. Some samples were later exposed to He plasma in the MAGPIE linear plasma device to a fluence of $1x10^{23}$ He-m^{-2} with an incident He ion energy of ~30 eV. All plasma exposures were performed at a He flux of $1.3x10^{21}$ He-m^{-2} s^{-1}. Due to the short exposure times, sample temperatures did not fully equilibrate during plasma exposure and remained within the range 300-400 K for all samples. A further three samples that had not been pre-irradiated with W ions were exposed to He plasma to fluences of $5x10^{23}$ He-m^{-2}, $8.5x10^{23}$ He-m^{-2}, and $1.2x10^{24}$ He-m^{-2}. For clarity, these experimental series are summarised in Table 1.

Table 1: Summary of sample treatments

Experiment name	1 MeV W-ion		He plasma fluence (He-m^{-2})
	Damage level (dpa)	Fluence (ions-m^{-2})	
Series-A	0.001 0.005 0.01 0.02 0.04	$1.8x10^{15}$ $9.0x10^{15}$ $1.8x10^{16}$ $3.6x10^{16}$ $7.2x10^{16}$	None for all samples

	0.05 0.1 0.15 0.2 0.3	$9.0x10^{16}$ $1.8x10^{17}$ $2.7x10^{17}$ $3.6x10^{17}$ $5.4x10^{17}$	
Series-B	0.04 0.05 0.1 0.15 0.2 0.3	$7.2x10^{16}$ $9.0x10^{16}$ $1.8x10^{17}$ $2.7x10^{17}$ $3.6x10^{17}$ $5.4x10^{17}$	$1.0x10^{23}$ for all samples
Series-C	None for all samples		$1.0x10^{22}$ $5.0x10^{22}$ $1.0x10^{23}$ $5.0x10^{23}$ $8.5x10^{23}$ $1.2x10^{24}$

Positron annihilation lifetime spectroscopy (PALS) was performed on all samples both after W-ion irradiation (Series-A), and again after He plasma exposure in MAGPIE (Series-B), using the positron beamline at the Australian National University [21]. Lifetime spectra were obtained for each irradiated and plasma exposed tungsten sample, and compared to the spectrum for an undamaged sample. Any difference appears as an additional lifetime component due to the damage induced in the sample. The beamline has a positron pulse width of ~0.9 ns, which allows for the resolution of lifetimes of as low as 0.2 ns, counting typically 3 million annihilation events in the case of the measurements presented here. The operation of the beamline and further details of the analysis procedure have been published previously [21]. PALS experiments were performed both with 3 keV and 11 keV positron beams in order to probe different depths within the material, as shown in Figure 1. A positron energy of 11 keV was selected to approximately overlap the implanted ion ranges predicted by SRIM [18] with greatest sensitivity to depth range 30-150 nm, while the 3 keV positron depth profile covers the first 30 nm where SRIM predicts many vacancies are generated but relatively few implanted ions terminate within this region. The first 30 nm is also where most He damage during plasma exposure is expected.

Figure 2 summarises the positron lifetime results for Series-A and Series-B described above. W-ion irradiated W samples (Series-A) probed with 11 keV positrons reveals an increase in positron lifetime with increasing W-ion fluence, from 0.153 ± 0.08 ns at 0.02 dpa to 0.32 ± 0.10 ns at 0.3 dpa. This corresponds to an increase in defect size from approximately a single vacancy (0.02-0.04 dpa) to clusters of 11-13 vacancies (0.2-0.3 dpa). These defect cluster sizes were estimated from the theoretical calculations presented in [22]. For the highest fluence samples, an additional long lifetime around 14-18 ns was also observed, which corresponds to the formation of significantly larger voids within the material. No change in positron spectra was observed for samples exposed to W-ion damage levels below 0.02 dpa.

After He plasma exposure (Series-B) positron lifetimes lie within the range 0.3-0.4 ns for all samples. This represents a significant increase in defect size for the 0.04 dpa W-ion exposed samples, but falls close to the error range of the 0.05, 0.1, and 0.2 samples. Comparing intensities between Series-A and Series-B reveals a significant drop in intensity at both low (0.04-0.05 dpa) and high (0.3 dpa) damage levels, as well as the complete elimination of the larger (>10 ns) lifetimes observed at 0.2-0.3 dpa. This reduction in intensity at 0.04-0.05 indicates partial filling of defects with He, which has the effect of reducing the lifetimes within the defects to below the detection limits of the PALS instruments used for this work. The corresponding lifetime increase for the 0.04 dpa sample exposed to He plasma suggests enhanced vacancy clustering also occurred after He exposure. Di-vacancies are known to be unstable in tungsten but can be stabilised through the addition of two or more helium atoms [7]. Thus, it is likely that the presence of helium enables vacancies to cluster into larger voids. The disappearance of the long (> 10 ns) lifetime observed at 0.2-0.3 dpa may also be a consequence of He filling, and could indicate that He preferentially fills these larger structures.

The reduction in the intensity of the shorter (< 1 ns) lifetime at 0.3 dpa is accompanied by an increase in the length of that lifetime. Due to the analysis techniques used for PALS measurements, there is some correlation between lifetime and intensity. Consequently, this does not necessarily mean more He filling occurred than for the 0.2 dpa sample. Instead, it is possible that some consolidation of vacancy clusters occurred, leading to the formation of a smaller number of larger clusters/voids within the sample.

Interestingly, 3 keV positron spectra for all samples in Series-A and Series-B are identical to that for the corresponding reference W sample. This indicates that no significant vacancy/void formation has occurred within the first ~30 nm of the sample surface. This is consistent with collision cascade modelling of W by [23] which suggests that for room temperature irradiation vacancy clusters smaller than ~10 vacancies recover shortly after the collision cascade due to thermal annealing. In W, primary knock-on energies >6 keV are necessary to create large enough vacancy clusters to survive this early-stage recovery [23]. This can be explained by the very high diffusivity of tungsten interstitials [24], which are mobile enough at room temperature to enable recombination with vacancies if the interstitials are not bound within a larger cluster. Figure 3a shows the depth dependence on the energies of PKAs for 1 MeV W-ion irradiated W, calculated by parsing the output from SRIM's full collision cascade calculation, with high energy (>6 keV) PKAs emphasised in Figure 3b. The proportion of high energy PKAs doesn't peak until a depth of ~45 nm, thus one could expect a significantly greater rate of residual damage accumulation at these greater depths. Quantifying this effect is difficult as there is a non-trivial relationship between PKA energy and residual damage, and collision cascades can overlap earlier damage.

For samples exposed to He plasma alone (Series-C) positron lifetimes on the order of 0.5-0.6 ns were observed for samples exposed to fluences of $5x10^{23}$ He-m^{-2} and higher with 3 keV positrons, likely due to nano-bubble formation (Figure 4). Defect formation was not observed for fluences $1x10^{23}$ He-m^{-2} and below. The absence of nano-bubbles for $1x10^{23}$ He-m^{-2} exposures is similar to the 3 keV positron results for Series-B. The sudden jump from no

defects at all to 0.5-0.6 ns positron lifetimes over only a 5 fold increase in plasma fluence may in fact be a temperature effect rather than a fluence one. In MAGPIE samples are heated by the plasma, so for short ($1x10^{23}$ He-m^{-2}) exposures the sample temperature will only rise a few tens of degrees. We can consider that the main mechanism for helium-vacancy cluster nucleation is the trap mutation process described in [10], whereby an interstitial helium cluster spontaneously ejects a tungsten atom from its lattice site. As an example, an activation energy of approximately 0.7 eV would be required for a cluster of 7 helium atoms to create a vacancy via this mechanism. Assuming an Arrhenius reaction rate, a rise in sample temperature from 300 K to 400 K would increase vacancy formation from these clusters by a factor of ~900. Subsequent growth of helium-vacancy clusters would also be significantly enhanced by this temperature rise. 11 keV positron measurements were not performed as most He damage was expected within the first 30 nm.

3. Bubble formation under He plasma exposure

To measure larger (>1 nm diameter) bubble formation grazing incidence small angle X-ray scattering (GISAXS) was performed on one sample that had been exposed to a helium fluence of $5x10^{23}$ He-m^{-2} (Sample-A) and a second that had been pre-irradiated with 0.04 dpa 1 MeV tungsten ions before $1x10^{23}$ He-m^{-2} fluence plasma exposure. GISAXS was performed at the SAXS/WAXS beamline of the Australian Synchrotron [25] with 10 keV X-rays and a camera length of 945 mm. GISAXS measurements were taken across a range of angles in order to probe how the sizes of bubbles changes with increasing depth within the sample.

GISAXS patterns were analysed using a Monte-Carlo fitting routine that was developed in-house. Bubbles were assumed to be spheroidal in shape with their axis of revolution lying parallel to the sample surface normal, hereafter referred to as the *z*-direction. The GISAXS model is described by Thompson *et al.* [26]. Both the diameter in the x-y plane and the z-height/x-y diameter ratios were randomly generated for 50,000 bubbles. Bubbles were randomly replaced with a new bubble with a randomised diameter and height/diameter ratio, with changes being accepted if they led to an improvement of the fit. Convergence was defined as the state when 250 consecutive bubble substitutions had been rejected.

An example of a GISAXS pattern and fit is shown in Figure 5. Figure 5a shows the contribution from surface scattering, which consists of a single bright streak running along the q_z axis. After helium exposure (Figure 5b) a bulge of intensity emerges about this bright streak due to the formation of sub-surface bubbles. The simulated pattern in Figure 5c shows the best fit of the pattern in 5b. Finally, the normalised residual (i.e. $1 - simulation/experiment$) for the fit is shown in Figure 5d, demonstrating excellent agreement between the experimental and simulated patterns. Note that no attempt was made to fit the surface scattering feature about q_y=0.

Figure 6 shows population distributions for nano-bubbles in both samples. To quantify subpopulations within these data a Gaussian mixture clustering algorithm [27] was used to divide nano-bubbles into 3 distinct categories, referred to here as “small”, “oblate”, and

“prolate” bubbles. Median bubble radii and height/width ratios for each cluster are represented by an “X”, while spreads of these distributions are represented graphically by a white line that encompasses 68% of the bubbles within that subpopulation. This classification method was selected as it aids in visualising the results.

For samples that have been pre-exposed to tungsten ion irradiation (Figure 6b) “small” bubbles show a much tighter distribution of height/width ratios, indicating bubbles are of a roughly uniform, near-spherical shape. Without tungsten ion pre-irradiation these “small” bubbles show a much greater variability in their shapes. This greater deviation from sphericity makes sense if one considers that without pre-irradiation to induce vacancies and other defects bubble nucleation will occur predominantly along grain boundaries or near the sample surface where there are significant material anisotropies, as predicted in [13].

Table 2: Median bubbles of each bubble population fit from cluster analysis.

	$5x10^{23}$ He-m^{-2}			0.04 dpa damage level 1 MeV W $1x10^{23}$ He-m^{-2}		
Bubble type	Small	Oblate	Prolate	Small	Oblate	Prolate
Fraction	0.807	0.131	0.062	0.839	0.110	0.051
Volume ($Å^3$)	782	4940	4380	882	6640	4530
Height/Diameter	0.95	0.51	1.38	0.91	0.58	1.33

Table 2 summarises the median bubbles for each of the “small”, “oblate” and “prolate” bubble populations determined from the cluster fitting process. Due to correlations between the radii and height/diameter ratios a full covariance matrix is necessary in order to gauge the scatter within these results. The white lines in Figure 6 are in effect a graphical representation of this, and present the most intuitive way of visualising the variability of each subpopulation.

Errors resulting from sources such as shot noise in the raw GISAXS data and Monte-Carlo sampling are negligible. However systematic errors, which are difficult to quantify, may be present. For rough guidance, previous work median bubble sizes calculated from GISAXS were found to agree with those determined by TEM within 15% [28].

For tungsten pre-exposed to 0.04 dpa 1 MeV tungsten ions there is a notable increase in median bubble sizes for all bubble classes, as well as significant increase in the proportion of “small” bubbles. The increase in the share of “small” bubbles supports the idea that the presence of tungsten-ion induced vacancies enhances the nucleation and growth rates of bubbles, without increasing the rate of bubble mergers that lead to the formation of “oblate” and “prolate” bubbles. This radiation-enhanced bubble formation is consistent with the PALS results that indicate a significant positron lifetime increase for the sample after helium plasma exposure at the fluence $1x10^{23}$ He-m^{-2}, despite no positron lifetimes being observed for $1x10^{23}$ He-m^{-2} fluence plasma exposure without pre-irradiation.

Due to attenuation within the material as X-rays propagate through tungsten, increasing the incident angle allows X-rays to penetrate deeper within the material. Consequently, it is possible to gain a qualitative understanding of how nano-bubble populations change as a

function of depth within the material by varying the incident angle of GISAXS measurements. Figure 7 shows how the median size of “small” bubbles changes as a function of the X-ray incident angle. For both samples the median volume of the bubbles decreases with increasing angle (and hence depth). This is consistent with the authors’ experience from TEM [28].

Notably, the drop in bubble size with measurement angle is significantly greater for the sample that had not been pre-exposed to tungsten ion radiation. This can be explained as follows. Vacancy formation energies in tungsten decrease markedly in the vicinity of the sample surface and defects such as grain boundaries [13], so for tungsten with few pre-existing vacancies bubble formation initially occurs predominantly within a few nanometres of the sample surface. Once bubbles form, they facilitate the nucleation of satellite bubbles in their vicinity by enhancing local trap mutation rates, as predicted by Perez *et al.* [29]. Consequently, a dense layer of bubbles will grow inwards from the surface. As shallower bubbles will tend to be older, bubble size decreases markedly with depth. Eventually, at high fluence, this dense bubble layer forms a diffusion barrier that prevents further uptake of helium, limiting the modification to the near-surface region of the material, as predicted by Krasheninnikov *et al.* [30].

For tungsten with a high initial vacancy concentration, for instance due to radiation damage, bubble nucleation can occur anywhere these vacancies are present, and their growth may be enhanced by the agglomeration of nearby vacancies. Shallower bubbles will be closer to the supply of incoming helium, so can be expected to be somewhat larger, but nucleation of deeper bubbles is not contingent on the formation of older bubbles above them. As a result, a less dramatic depth dependence on bubble formation is expected.

This interpretation has significant implications for the operation of the divertor in the presence of neutron irradiation as it suggests that the volume of material modified by helium from the plasma could be substantially greater than predicted by plasma studies alone.

4. Conclusions

Positron annihilation lifetime spectroscopy was performed on tungsten samples exposed to 1 MeV tungsten ions across a range of damage levels (0.001-0.3 dpa). Vacancies clusters were not observed within the first 30 nm of the sample surface in any of these samples. This indicates efficient vacancy-interstitial recombination, which we suggest is a consequence of the high mobility of tungsten interstitials [24] and instability of tungsten di-vacancies [7]. At greater depths (30-150 nm) vacancy clusters formed, and were found to increase in size with increasing W-ion fluence. This indicates that vacancy clusters are stabilised somehow, possibly due to the higher energies expected for collision cascades at these depths leading to the formation of larger clusters. No vacancy formation was observed for samples with damage levels of 0.01 dpa or lower with either 3 keV or 11 keV positrons.

These self-implanted samples were then exposed to helium plasma in the MAGPIE linear plasma device at ~300 K and a fluence 10^{23} He-m^{-2}. After plasma exposure deeper (30-150 nm) vacancy clusters showed similar positron lifetimes (0.3-0.4 ns), while shallow (<30 nm)

clusters were not observed. Positron lifetime intensities fell for most samples after plasma exposure, possibly indicating that defects were filling with helium. The absence of shallow clusters indicates that helium requires pre-existing defects in order to drive vacancy cluster growth at 300 K.

Further samples that had not been pre-damaged with W-ions were also exposed to helium plasma in MAGPIE across fluences from $1x10^{22}$ to $1.2x10^{24}$ He-m^{-2}. PALS measurements were performed using 3 keV positrons, as most plasma-induced damage is expected in this region. Samples exposed to fluences up to $1x10^{23}$ He-m^{-2} showed no signs of damage. This resembles the behaviour to the 1 MeV W implanted samples which also showed no change in the first 30 nm after $1x10^{23}$ He-m^{-2} plasma fluence. Fluences of $5x10^{23}$ He-m^{-2} and higher showed significant helium-cluster formation within the first 30 nm, with positron lifetimes in the vicinity 0.5-0.6 ns. The sample temperature was significantly higher for these higher fluence exposures (~400 K) due to plasma heating. This higher temperature likely enhanced bubble formation by significantly increasing the rate interstitial helium clusters generate vacancies.

GISAXS results show that bubble sizes decrease with increasing distance from the tungsten surface for samples exposed to helium plasma, both with and without pre-irradiation with tungsten ions. The reduction in bubble size with depth is much more significant for the sample that had not been pre-irradiated with tungsten ions, possibly indicating that in the absence of vacancies to serve as nucleation sites bubbles tend to form near the surface where vacancy formation energies are lower, and grow inward. Where pre-existing radiation damage is present bubbles can nucleate from radiation-induced defects such as vacancies, so bubble formation is less sensitive to the distance from the surface.

Acknowledgements

The authors are grateful to the technical assistance within the Australian Plasma Fusion Research Facility that is partly funded by the Australian Government under the Super Science Initiative, financed from the Education Investment Fund. GISAXS work was conducted on the SAXS/WAXS beamline of the Australian Synchrotron with support from the Australian Synchrotron Access Program, AS163/SAXS/11328. We gratefully acknowledge beamline scientists at the Australian Synchrotron for their assistance. PK acknowledges the Australian Research Council for financial support.

References

[1] J. Marian, C.S. Becquart, B.D. Wirth, E.M. Bringa, A Kinetic Monte Carlo Model for Helium Diffusion and Clustering in Fusion Environments Related content Recent advances in modeling and simulation of the exposure and response of tungsten to fusion energy conditions A Kinetic Monte Carlo Model for Helium Diffusion and Clustering in Fusion Environments, Phys. Scr. (2004). http://iopscience.iop.org/article/10.1238/Physica.Topical.108a00080/pdf (accessed October 12, 2017).

[2] Z. Yang, S. Blondel, K.D. Hammond, B.D. Wirth, Kinetic Monte Carlo Simulations of Helium Cluster Nucleation in Tungsten with Preexisting Vacancies, Fusion Sci. Technol. 71 (2017) 60–74. doi:10.13182/FST16-111.

[3] A.V. Barashev, H. Xu, R.E. Stoller, The behavior of small helium clusters near free surfaces in tungsten, J. Nucl. Mater. 454 (2014) 421–426. doi:10.1016/j.jnucmat.2014.08.033.

[4] N. Fernandez, Y. Ferro, D. Kato, Hydrogen diffusion and vacancies formation in tungsten: Density Functional Theory calculations and statistical models, Acta Mater. 94 (2015) 307–318. doi:10.1016/j.actamat.2015.04.052.

[5] S.C.C. Middleburgh, R.E.E. Voskoboinikov, M.C.C. Guenette, D.P.P. Riley, Hydrogen induced vacancy formation in tungsten, J. Nucl. Mater. 448 (2014) 270–275. doi:10.1016/j.jnucmat.2014.02.014.

[6] A. Satta, F. Willaime, S. De Gironcoli, Vacancy self-diffusion parameters in tungsten: Finite electron-temperature LDA calculations, (1997). https://journals.aps.org/prb/pdf/10.1103/PhysRevB.57.11184 (accessed August 22, 2017).

[7] C.S. Becquart, C. Domain, An object Kinetic Monte Carlo Simulation of the dynamics of helium and point defects in tungsten, J. Nucl. Mater. 385 (2009) 223–227. doi:10.1016/j.jnucmat.2008.11.027.

[8] K.O.E. Henriksson, K. Nordlund, A. Krasheninnikov, J. Keinonen, Difference in formation of hydrogen and helium clusters in tungsten, Appl. Phys. Lett. 87 (2005). doi:http://dx.doi.org/10.1063/1.2103390.

[9] W.D. Wilson, C.L. Bisson, M.I. Baskes, Self-trapping of helium in metals, Phys. Rev. B. 24 (1981) 5616–5624. doi:10.1103/PhysRevB.24.5616.

[10] D. Perez, T. Vogel, B.P. Uberuaga, Diffusion and transformation kinetics of small helium clusters in bulk tungsten, Phys. Rev. B. (2014) 14102. doi:10.1103/PhysRevB.90.014102.

[11] D. Perez, L. Sandoval, S. Blondel, B.D. Wirth, B.P. Uberuaga, A.F. Voter, The mobility of small vacancy/helium complexes in tungsten and its impact on retention in fusion-relevant conditions, Sci. Rep. 7 (2017) 2522. doi:10.1038/s41598-017-02428-2.

[12] L. Hu, K.D. Hammond, B.D. Wirth, D. Maroudas, Dynamics of small mobile helium clusters near tungsten surfaces, Surf. Sci. 626 (2014) L21–L25. doi:10.1016/j.susc.2014.03.020.

[13] L. Hu, K.D. Hammond, B.D. Wirth, D. Maroudas, Interactions of mobile helium clusters with surfaces and grain boundaries of plasma-exposed tungsten, J. Appl. Phys. 115 (2014) 173512. doi:10.1063/1.4874675.

[14] M.S. Abd El Keriem, D.P. van der Werf, F. Pleiter, Helium Vacancy Interaction in Tungsten, Phys. Rev. B. 47 (1993) 14771–14777.

[15] J. Wang, L.-L. Niu, X. Shu, Y. Zhang, Energetics and kinetics unveiled on helium cluster growth in tungsten, Nucl. Fusion. 55 (2015) 92003. doi:10.1088/0029-5515/55/9/092003.

[16] K.D. Hammond, S. Blondel, L. Hu, D. Maroudas, B.D. Wirth, Large-scale atomistic simulations of low-energy helium implantation into tungsten single crystals, Acta Mater. 144 (2018) 561–578. doi:10.1016/J.ACTAMAT.2017.09.061.

[17] X. Hu, T. Koyanagi, M. Fukuda, Y. Katoh, L.L. Snead, B.D. Wirth, Defect evolution in single crystalline tungsten following low temperature and low dose neutron irradiation, J. Nucl. Mater. 470 (2016) 278–289. doi:10.1016/J.JNUCMAT.2015.12.040.

[18] J.F. Ziegler, M.D. Ziegler, J.P. Biersack, {SRIM} – The stopping and range of ions in matter (2010), Nucl. Instruments Methods Phys. Res. Sect. B Beam Interact. with Mater. Atoms. 268 (2010) 1818–1823. doi:http://dx.doi.org/10.1016/j.nimb.2010.02.091.

[19] R.E. Stoller, M.B. Toloczko, G.S. Was, A.G. Certain, S. Dwaraknath, F.A. Garner, On the use of SRIM for computing radiation damage exposure, Nucl. Instruments Methods Phys. Res. Sect. B Beam Interact. with Mater. Atoms. 310 (2013) 75–80. doi:10.1016/j.nimb.2013.05.008.

[20] American Society for Testing and Materials, Standard Practice for Neutron Radiation Damage Simulation by Charge-Particle Irradiation, E521-96, Annual Book of ASTM Standards, vol. 12.02, Philadelphia, 1996.

[21] J.P. Sullivan, J. Roberts, R.W. Weed, M.R. Went, D.S. Newman, S.J. Buckman, A trap-based positron beamline for the study of materials, Meas. Sci. Technol. 21 (2010) 85702. doi:10.1088/0957-0233/21/8/085702.

[22] T. Troev, E. Popov, P. Staikov, N. Nankov, T. Yoshiie, Positron simulations of defects in tungsten containing hydrogen and helium, Nucl. Instruments Methods Phys. Res. Sect. B Beam Interact. with Mater. Atoms. 267 (2009) 535–541. doi:10.1016/j.nimb.2008.11.045.

[23] J.R. Beeler, Displacement Spikes in Cubic Metals. I. α -Iron, Copper, and Tungsten, Phys. Rev. 150 (1966) 470–487. doi:10.1103/PhysRev.150.470.

[24] T.D. Swinburne, P.-W. Ma, S.L. Dudarev, Low temperature diffusivity of self-interstitial defects in tungsten, New J. Phys. 19 (2017) 73024. doi:10.1088/1367-2630/aa78ea.

[25] N.M. Kirby, S.T. Mudie, A.M. Hawley, D.J. Cookson, H.D.T. Mertens, N. Cowieson, V. Samardzic-Boban, IUCr, K. N., M. S., P.A. G., L.K. S., G. A., K.M.H. J., A low-background-intensity focusing small-angle X-ray scattering undulator beamline, J. Appl. Crystallogr. 46 (2013) 1670–1680. doi:10.1107/S002188981302774X.

[26] M. Thompson, R. Sakamoto, E. Bernard, N. Kirby, P. Kluth, D. Riley, C. Corr, GISAXS modelling of helium-induced nano-bubble formation in tungsten and comparison with TEM, J. Nucl. Mater. 473 (2016) 6–12. doi:10.1016/j.jnucmat.2016.01.038.

[27] F. Pedregosa, G. Varoquaux, A. Gramfort, V. Michel, B. Thirion, O. Grisel, M. Blondel, P. Prettenhofer, R. Weiss, V. Dubourg, J. Vanderplas, A. Passos, D. Cournapeau, M. Brucher, M. Perrot, E. Duchesnay, Scikit-learn: Machine Learning in {P}ython, J. Mach. Learn. Res. 12 (2011) 2825–2830.

[28] M. Thompson, R. Sakamoto, E. Bernard, N. Kirby, P. Kluth, D. Riley, C. Corr, GISAXS modelling of helium-induced nano-bubble formation in tungsten and comparison with TEM, J. Nucl. Mater. 473 (2016) 6–12. doi:10.1016/j.jnucmat.2016.01.038.

[29] D. Perez, L. Sandoval, B.P. Uberuaga, A.F. Voter, The thermodynamic and kinetic interactions of He interstitial clusters with bubbles in W, J. Appl. Phys. 119 (2016) 203301. doi:10.1063/1.4951706.

[30] S.I. Krasheninnikov, T. Faney, B.D. Wirth, On helium cluster dynamics in tungsten plasma facing components of fusion devices, Nucl. Fusion. 54 (2014) 73019. doi:10.1088/0029-5515/54/7/073019.

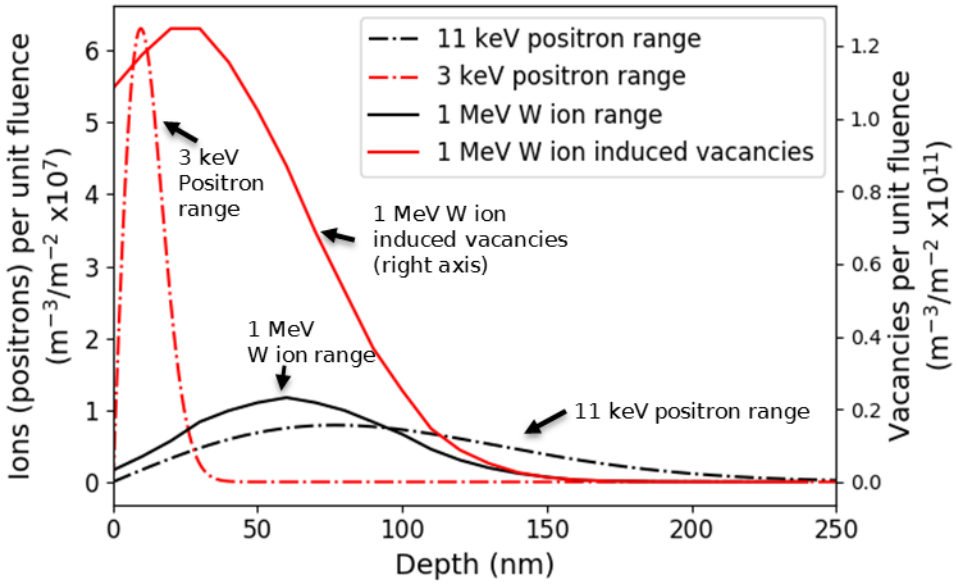

Figure 1: Comparison of 3 keV and 11 keV positron implantation profiles, and W ion implantation profiles and vacancy profiles predicted by SRIM [18]. *The 3 keV positron profile covers the first 30 nm where the W ion implantation profile is relatively low, but vacancies are expected to be abundant, while the 11 keV positron profile roughly overlaps the ion range profile.*

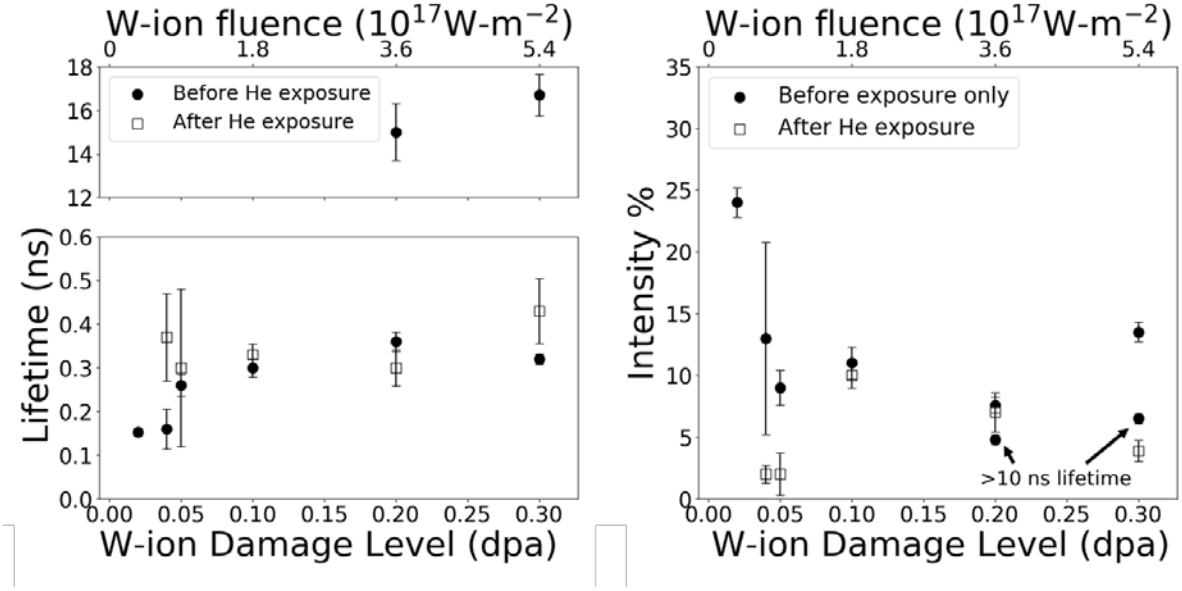

Figure 2: (left) Positron lifetimes for 11 keV positron studies of samples implanted with 1 MeV W-ions to a range of fluences both before (Series-A, solid circles) and after (Series-B, open squares) He plasma exposure, along with (right) relative intensities of these positron lifetimes. The presence of He leads to a significant reduction in positron intensities due to defects filling with He. This effect is especially strong at lower damage rates.

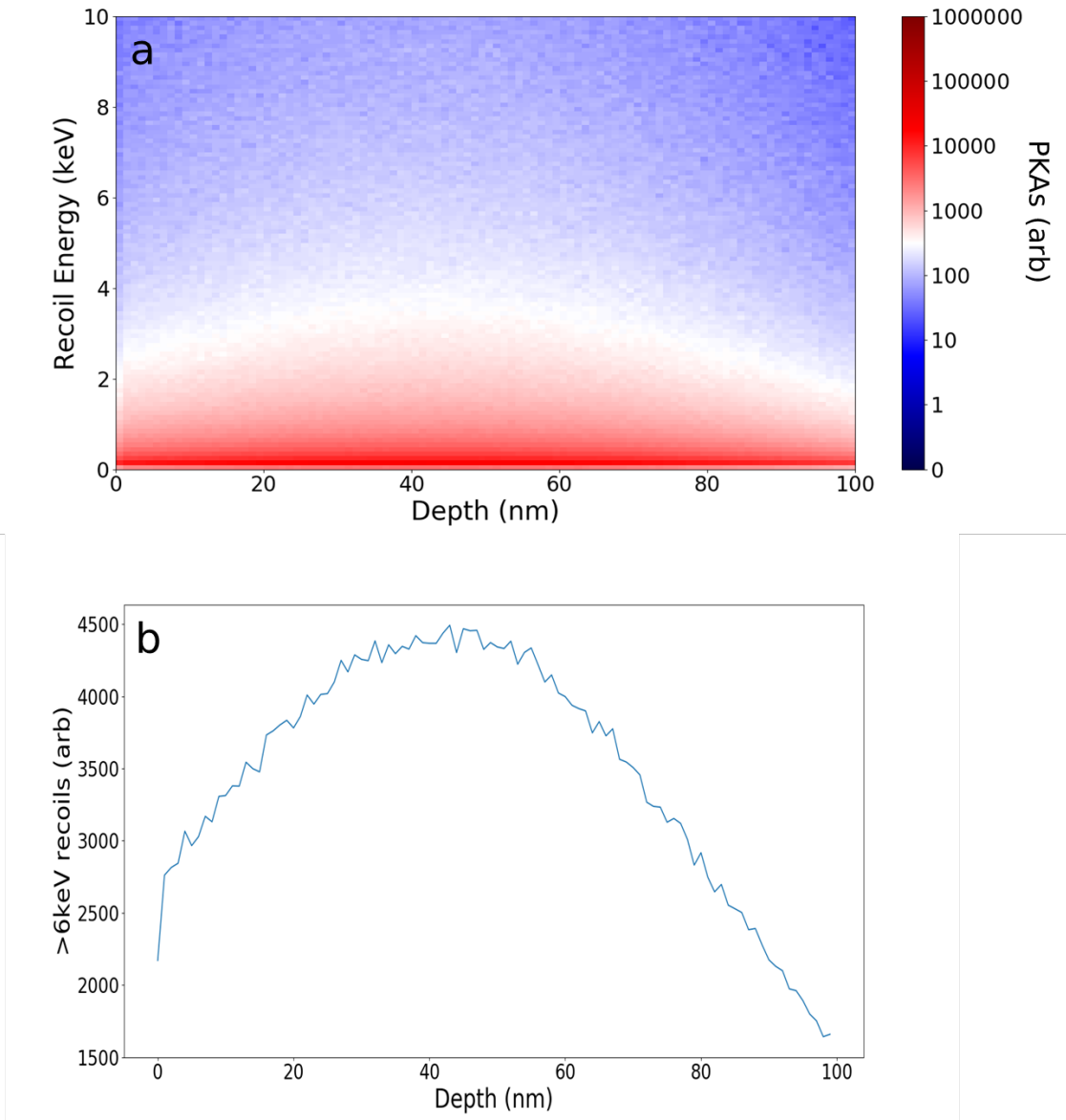

Figure 3: (a) PKA energy dependence for 1 MeV W implanted into W at room temperature as a function of depth, and (b) relative proportion of PKAs that have energies in excess of 6 keV as a function of depth. Vacancies produced by higher energy recoils are more likely to survive the lattice relaxation that occurs after ion implantation.

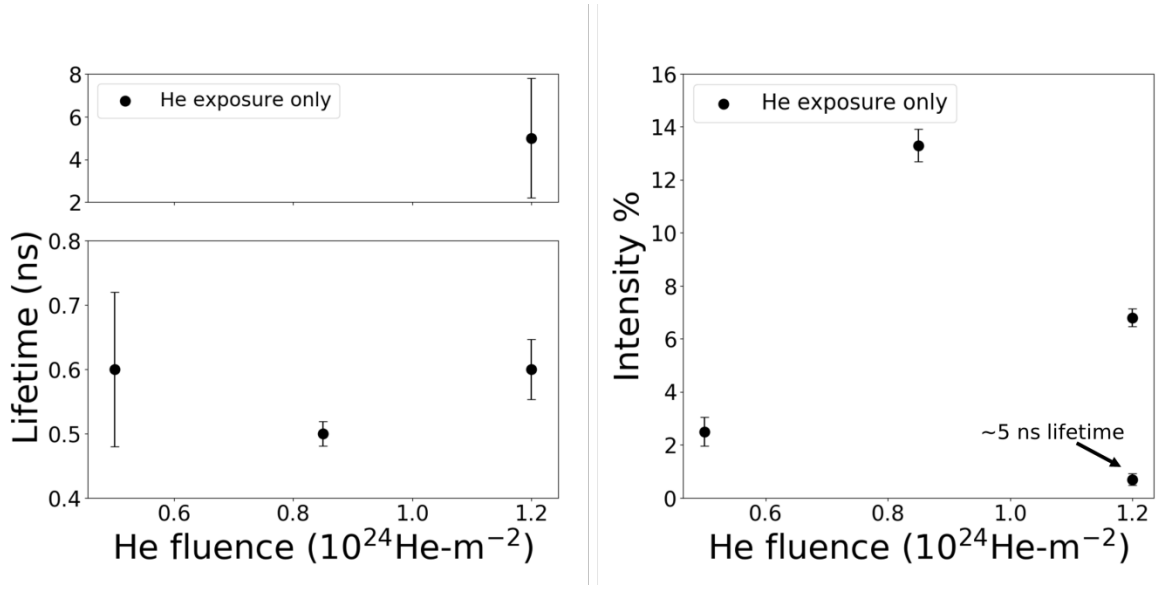

Figure 4: (left) Positron lifetimes for 3 keV positrons implanted into W exposed to He plasma (Series C) across a range of fluences, and (right) corresponding intensities for these measurements.

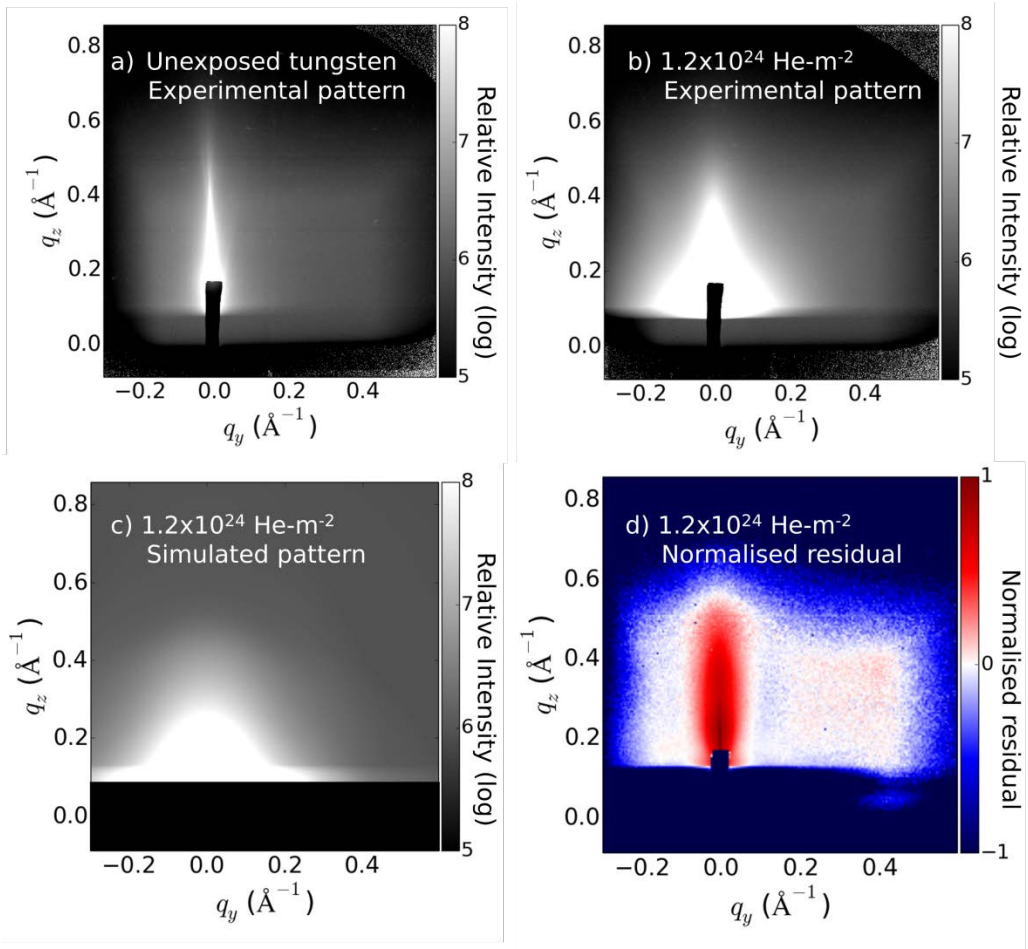

Figure 5: (a) Experimental GISAXS pattern for an unexposed sample, (b) experimental GISAXS pattern for sample exposed to 1.2×10^{24} *He-m^{-2} plasma, (c) simulated GISAXS pattern for the best fit of (b), and (d) the normalised residual of the fit. The streak near q_y=0 is caused by surface scattering and was not fitted.*

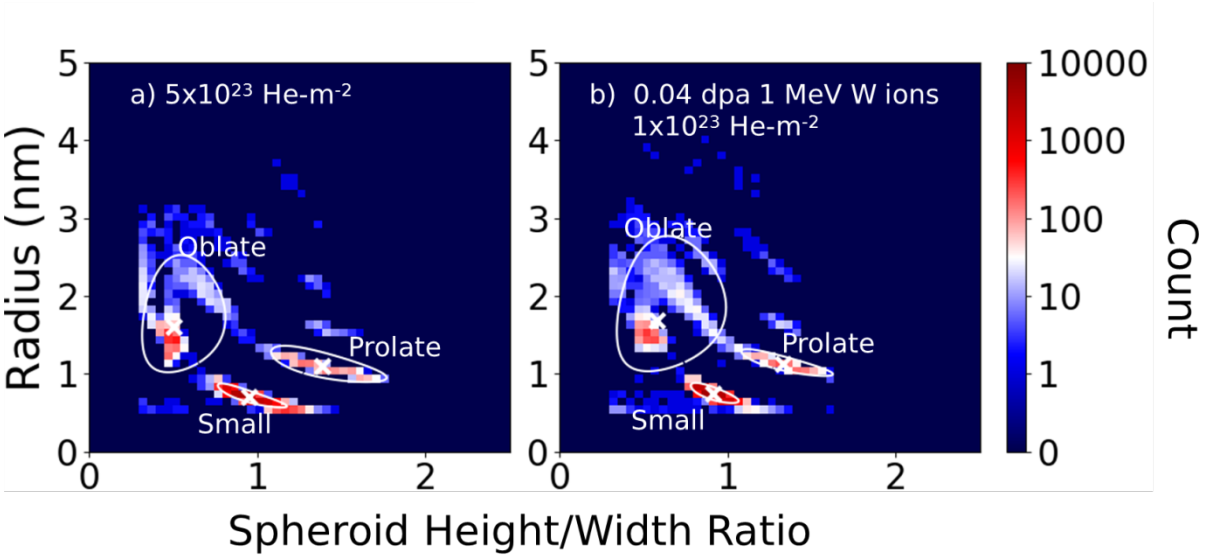

Figure 6: Population distributions of spheroidal nano-bubble radii and height/width ratios for tungsten (a) exposed to 5x10^{23} He-m^{-2} fluence He plasma and (b) 0.04 dpa 1 MeV W ions prior to 1x10^{23} He-m^{-2}. Measurements were taken for a grazing incidence angle of 1.0°.

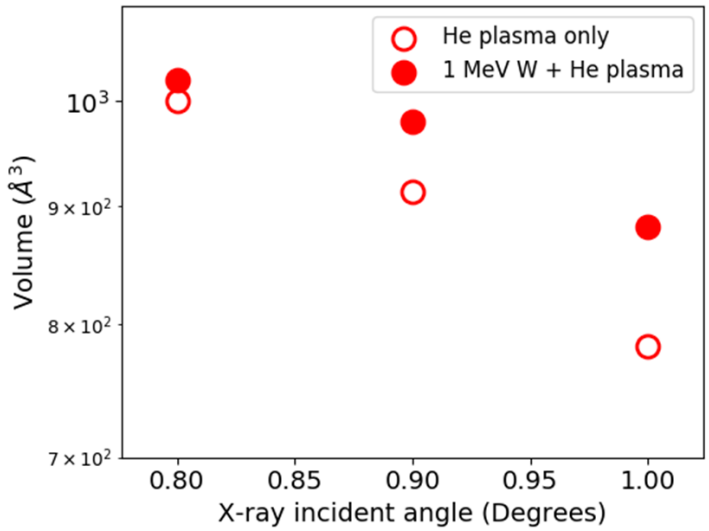

Figure 7: Median "small" bubble volumes computed from GISAXS measurements taken at different incident angles. The greater the angle, the deeper X-rays are able to probe into the material, providing some qualitative indication of how bubble populations change with depth.